Journal of Hydrology 574 (2019) 1099–1109

Contents lists available at ScienceDirect

Journal of Hydrology

journal homepage: www.elsevier.com/locate/jhydrol

Research papers

Saline water intrusion in relation to strong winds during winter cold outbreaks: North Branch of the Yangtze Estuary

Erfeng Zhang[a,*], Shu Gao[a,*], Hubert H.G. Savenije[b], Cunyou Si[c], Shuai Cao[c]

[a] State Key Laboratory of Estuarine and Coastal Research, East China Normal University, Shanghai 200241, China
[b] Department of Water Management, Delft University of Technology, Delft 2600 GA, Netherlands
[c] Jiangsu Province Hydrology and Water Resources Investigation Bureau, Nanjing 210029, China

ARTICLE INFO

This manuscript was handled by Dr. A. Bardossy, Editor-in-Chief, with the assistance of Qiuhua Liang, Associate Editor

Keywords:
Saline water intrusion
Strong winds
Cold outbreaks
Yangtze Estuary

ABSTRACT

The strong saline water intrusion in the North Branch of the Yangtze Estuary threatens the freshwater supply of the region in winter half year. Strong northerly winds have been identified as a factor increasing saline water intrusion. However, there are few studies on this subject, and the mechanisms of winds influencing saline water intrusion are still unclear. In the present contribution, we investigate the variation trend of strong wind events during cold outbreaks in winter half year and their correlation with saline water intrusion in the North Branch, together with the processes and mechanism of strong winds increasing saline water intrusion, based on observations and an analytical salt water intrusion model. The results indicate that the strong northerly and northeasterly wind events and saline water intrusion in the North Branch have similar variation trends in 1994–2008, both being relatively weak in the 1990s but being intensified dramatically after 1999. The significant correlation between these two trends suggests that the increase in strong wind events may be one of the factors inducing the enhanced saline water intrusion. Observations and model output show that the strong northerly and northeasterly winds can induce dramatic water level setup, increase of flood-tide current velocities, decrease of ebb-tide velocities, and decrease of freshwater inflow into the North Branch. These changes in combination cause the enhanced intensity of saline water intrusion. The Ekman transport from remote winds results in water level setup at the estuary mouth pumping more seawater into the North Branch, which should be a dominant mechanism inducing the change in hydrodynamics and increase of saline water intrusion.

1. Introduction

In non-tidal and micro-tidal estuaries, wind can significantly affect hydrodynamics and salt transport. In recent decades many scholars have researched the effects of wind on the subtidal variability and salinity regime in estuaries and bays over the Atlantic Ocean and the Mediterranean Sea, e.g., Great South Bay (Wong and Wilson, 1984), Delaware Estuary (Wong and Garvine, 1984; Wong and Moses-Hall, 1998), Lower Patos Lagoon Estuary (Costa et al., 1988), Hudson River Estuary (Ralston et al., 2008), Rio de la Plata Estuary (Simionato et al., 2007), Pamlico River Estuary (Xu et al., 2008), St. Johns River Estuary (Giardino, 2009), Atchafalaya Bay (Li et al., 2011), and Tiber river mouth (Manca et al., 2014). In meso-tidal and macro-tidal estuaries, river discharge and tidal dynamics are believed to represent the primary forcing. The effects of wind are usually ignored and there are few related studies, including those by Bolaños et al. (2013), on the influence of wind on the circulation of the Dee, a macro-tidal estuary, and by Reyes-Merlo et al. (2015), on the impacts of wind conditions on the salt intrusion in the Guadalquivir, a meso-tidal estuary.

The Yangtze Estuary is a meso-tidal, partially mixed estuary with complex topography: three-order bifurcations and four outlets towards the sea (Fig. 1). Among the branches the North Branch is a tidally dominated, well-mixed channel. Due to its special topography, i.e., almost perpendicular to the main channel South Branch and the trumpet channel shape, the freshwater inflow ratio is very small and the tidal range is large, resulting in the strongest saline water intrusion among the branches. In dry season the saline water in the North Branch often spill over into the South Branch during spring and intermediate tides, which is the main problem threatening freshwater supply around the estuary because there are several reservoirs for urban water supply along the South Branch.

River discharge, tidal intensity and topography interact controlling the saline water intrusion pattern in the North Branch of the Yangtze Estuary. In recent years strong winds were also found as a factor

* Corresponding authors.
E-mail addresses: efzhang@sklec.ecnu.edu.cn (E. Zhang), sgao@sklec.ecnu.edu.cn (S. Gao).

https://doi.org/10.1016/j.jhydrol.2019.04.096
Received 14 January 2019; Received in revised form 1 April 2019; Accepted 30 April 2019
Available online 03 May 2019

Fig. 1. Satellite imagery showing the general configuration of the Yangtze Estuary.

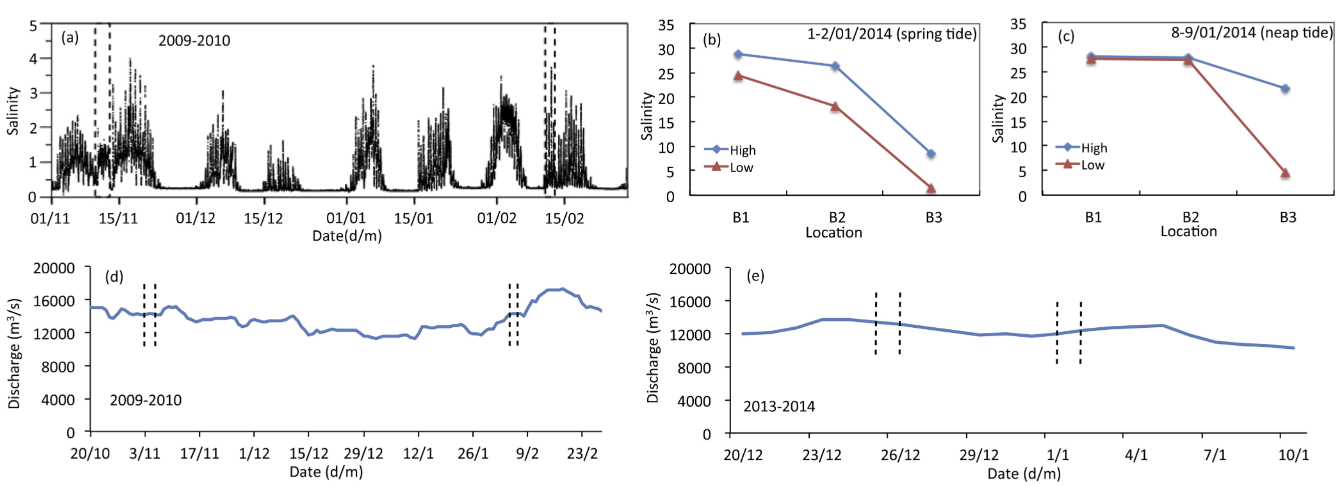

Fig. 2. Salinity at the Chongxi station between November 2009 and February 2010 (plot a), and salinity distribution in the North Branch on 1–2 and 8–9 January 2014 (plots b and c). The plot of salinity at the Chongxi station (plot a) is from Li et al. (2012), in which the salinities between dashed lines are the abnormal ones. Plots d and e show river discharges at the Datong station. The values between dashed lines, 7 days in advance, are the corresponding discharges.

influencing saline water intrusion. Li et al. (2012) found abnormal salinity increases at the Chongxi station, a fixed station measuring salinity located at the northern bank of the South Branch, during 10–12 November 2009 (neap tide) and 11–12 February 2010 (intermediate tide) (plot a in Fig. 2). The saline water at Chongxi originated from the North Branch. In January 2014 Zhang et al. (2014) also observed a strange phenomenon: saline water intrusion in the North Branch during neap tide was much stronger than during spring tide (plots b and c in Fig. 2). It can be seen from plot d in Fig. 2 that during and around the neap tide on 10–12 November 2009 the corresponding river discharges at Datong station (the values between dashed lines, 7 days in advance) were almost the same, i.e. around 14200 m^3/s, but the salinity at Chongxi increased suddenly during 10–12 November 2009. The discharges 7 days in advance were used because Datong is located some 700 km upstream of the river mouth, and 6–9 days are usually regarded as the time required for water to travel from Datong to the estuary (Xu and Yuan, 1994; Gu et al., 2003; Cao et al., 2006; Li et al., 2012; Zhang et al., 2012). During the intermediate tide on 11–12 February 2010, the river discharges were larger than during the neighboring neap tide and previous intermediate and spring tides, but the salinity at Chongxi increased sharply as well, even higher than during the previous spring tide. During the neap tide on 8–9 January 2014 the corresponding river discharges were similar to the spring tide on 1–2 January (the values between dashed lines in plot e of Fig. 2); however, the salinity along the North Branch was much higher than during spring tide. Both Li et al. (2012) and Zhang et al. (2014) proposed that the strong northerly winds were responsible for the abnormal salinity increases.

Wind patterns around the Yangtze Estuary show East Asian monsoon characteristics. The northerly winds are the prevailing winds in winter half year particularly between November and March, resulting from the passages of cold wave and strong cold air. This period is exactly in accordance with the strong saline water intrusion in the Yangtze Estuary. In terms of the effects of wind, there have been few related studies. Xue et al. (2009), Wu et al. (2010), and Li et al. (2012) carried out numerical experiments to study the effects of wind on the saline water intrusion. Li et al. (2012) modeled the abnormal salinity at Chongxi station during 10–12 November 2009 and 11–12 February 2010, and investigated the impacts of wind direction and speed on saltwater intrusion. Zhang et al. (2014) presented the observations of abnormally strong saline water intrusion during neap tide on 8–9 January 2014 compared with the spring tide, and discussed the impact factors. Most studies were based on numerical experiments, using average wind conditions, which is different from the real situation. The processes of winds affecting saline water intrusion, or how do the factors controlling saline water intrusion change influenced by winds are still poorly understood. In the Yangtze Estuary, the strong winds should be most important, could induce obvious effects. The aim of this study is to investigate the variation trend of strong wind events in winter half year and their correlation with saline water intrusion in the North Branch, and to reveal the processes and mechanism of strong winds increasing saline water intrusion, based on observations and model analysis.

2. Data sets used in the study

The data used in this study include salinity, river discharge, tidal level, wind observations, temperature, tidal current velocity, and water depth. The salinity, tidal current velocities and wind conditions at locations B1, B2 and B3 were measured on 1–2 and 7–9 January 2014. The river discharges at the Datong station were provided by the Hydrological Administration of Anhui Province. The tidal levels at the Qinglonggang station were provided by the Jiangsu Province Hydrology and Water Resources Investigation Bureau. The wind observations, the average speed and direction within 2 min, with intervals of three hours at the Shengsi station in 1994–2008 were obtained from the National Centers for Environmental Information (NCEI). The frequency and total durations of saline water intrusion at the Chenhang reservoir in 1994–2008 are from paper of Tang et al. (2011). The temperature with intervals of three hours at Shengsi in November 2009, February 2010, and January 2014 were obtained from the National Centers for Environmental Information (NCEI) as well. The wind observations, the average speed and direction within 2 min, with intervals of one hour at the Dongtan station in November 2009, February 2010, and January 2014 were obtained from the State Key Laboratory of Estuarine and Coastal Research. Water depths of the North Branch measured in 2012 were obtained from the State Key Laboratory of Estuarine and Coastal Research. The stations and locations of measurements are shown in Fig. 1.

3. Methods of analyses

3.1. Processing of tidal level and tidal range data

For eliminating sharp tidal oscillations with a period shorter than 25 h, the low-pass filter was used to obtain subtidal water levels and tidal ranges. In order to obtain the net setup and setdown of water level and tidal range affected by winds excluding other factors, the EMD (empirical mode decomposition) method was used to decompose tidal levels and tidal ranges.

3.1.1. The EMD method

The EMD (empirical mode decomposition) method was proposed by Huang et al. (1998). The processes are as follows. The first step is to identify the extrema, all the local maxima and minima from the original data. All the local maxima are connected by a cubic spline line as the upper envelope, and all the local minima are connected by a cubic spline line as the lower envelope. The upper and lower envelopes should cover all the data between them. Their mean is designated as m_1, and the difference between the data and m_1 is the first component, h_1, i.e.

$$X(t) - m_1 = h_1 \tag{1}$$

In the second sifting process, h_1 is treated as the data, then

$$h_1 - m_{11} = h_{11} \tag{2}$$

This sifting procedure is repeated for j times,

$$h_{1(j-1)} - m_{1j} = h_{1j} \tag{3}$$

Then $c_1 = h_{1j}$ is the first IMF (intrinsic mode function) component from the data. c_1 is separated from the data by

$$X(t) - c_1 = r_1 \tag{4}$$

The residue r_1 is treated as the new data and subjected to the same sifting process as described above. This procedure can be repeated on all the subsequent r_is, and the result is

$$r_1 - c_2 = r_2,\ ...,r_{(n-1)} - c_n = r_n \tag{5}$$

Finally, we obtain n IMF components and residue r_n, $X(t) = c_1 + c_2 + c_3 + \cdots + c_n + r_n$.

The IMF should have two properties: (1) throughout the whole length of a single IMF, the number of extrema and the number of zero-crossings must either be equal or differ at most by one; and (2) at any data location, the mean value of the envelope defined by the local maxima and the envelope defined by the local minima is zero. The total number of IMFs of a data set is close to and might be fewer than $\log_2 N$ with N the number of total data points (Wu and Huang, 2009).

There are two factors influencing the results. One is stopping criterion of producing an IMF component. The stopping criterion for the sifting used in the decompositions is a modified Cauchy-type criterion $C_r = \sum_i m_{ij}^2 / \sum_i h_{ij}^2$, where h_{ij} is the prototype ith IMF after j rounds of sifting, and m_{ij} is the mean of the upper and lower envelopes of h_{ij}. In the decompositions, a value of 0.0001 was selected for C_r (Wu and

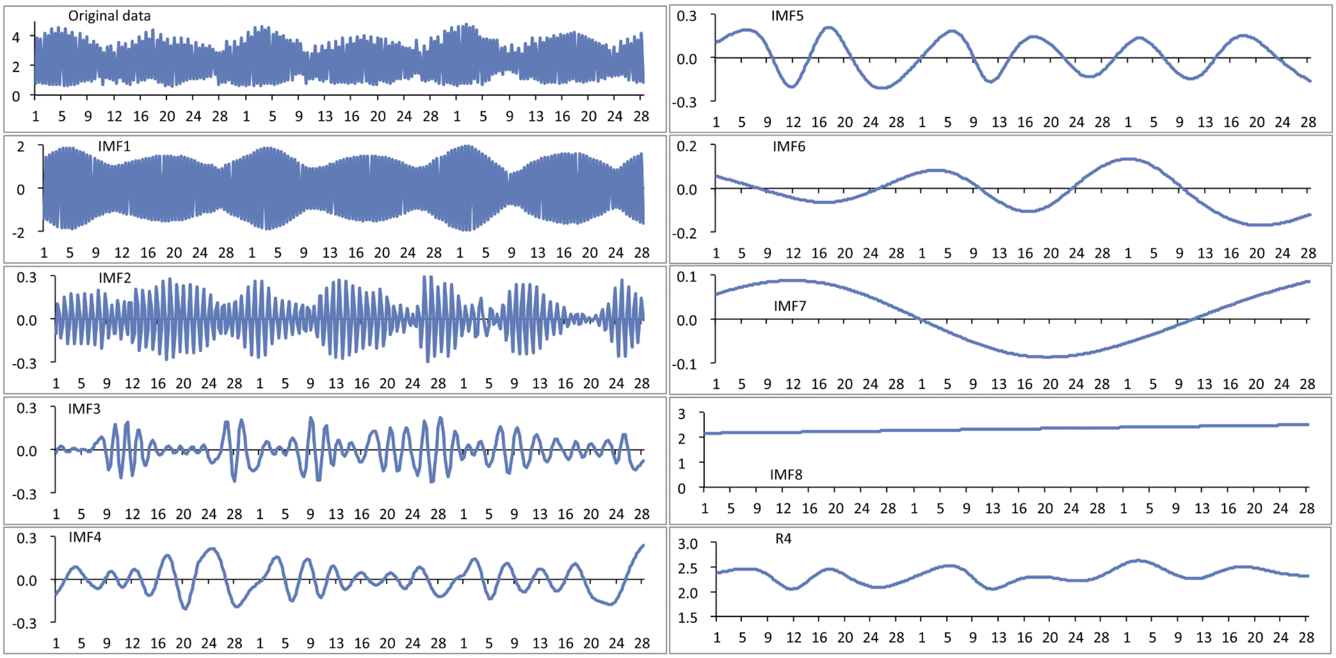

Fig. 3. EMD results of tidal levels between December 2013 and February 2014.

Huang, 2009). The other factor influencing the decomposed results is the end effects. We use the similar method proposed by Wu and Huang (2009) to reduce the end effects. In addition, we extended the data at two sides respectively, which is the best way resolving this problem.

3.1.2. Obtaining net setup and setdown of water level and tidal range

Taking tidal levels in January 2014 for example, eight IMF components are obtained after decomposition, which are presented in Fig. 3. IMF1 and IMF2 are clearly the components of semi-diurnal tides and diurnal tides, respectively. IMF5 is the component of half-monthly variation of tides. Its peaks and valleys are in accordance with spring tides and neap tides, respectively. IMF6 is the component of monthly variation of tides. Its peaks and valleys correspond with the relatively strong and weak spring tides, respectively. Because there are errors at the two sides, i.e. the end effects, the correspondence is relatively poor at the two sides. IMF7 and IMF8 should represent longer periodic variations. Therefore, IMF3 and IMF4 between diurnal tide component and half-monthly tide component should contain components of wind effects. The previous studies showed that 2–3 and 4–5 days are the main periods of low frequency variations of water level around the Yangtze Estuary, which are in accordance with the wind's variations (Zhao and Cao, 1987; Chen and Su, 1991). The IMF3 and IMF4 components correspond to the 2–3 days and 4–5 days periods, respectively. The sum of IMF3 and IMF4 is regarded as the net water level setup and setdown. The situation for November 2009 was a little bit different. The subtidal water levels were abnormal relative to the normal tidal variations, low in spring tide and high in neap tide, because the water level setdown and setup exactly occurred in spring tide and neap tide respectively, which can be seen from plot a in Fig. 7. The half-monthly tide and monthly tide components are not correctly decomposed, with peaks and valleys in neap tide and spring tide respectively, the same as the subtidal water levels. Therefore, IMF 5 and IMF 6 are included as well to obtain the net water level setup. For the tidal range, since all data looked normal, the same as the tidal variation, the data processing was similar to that for the tidal level.

3.2. Analytical model for saline water intrusion

For better analyzing the process of wind's effects on the saline water intrusion, an analytical model for alluvial estuaries developed by Savenije (1986, 1989, 2005) was used. This model has been successfully applied to the Yangtze Estuary by Zhang et al. (2011).

3.2.1. Summary of the model

The shape of alluvial estuaries can be described by the following exponential functions in a multiple-reach estuary. In estuaries where the geometry of channels cannot be described by a single exponential function, multiple reaches can be used.

$$A_i = A_0 \exp(-x/a_i)(i = 1),$$

$$A_i = A_{(i-1)} \exp(-(x - x_{(i-1)})/a_i)(i > 1) \quad (6)$$

$$B_i = B_0 \exp(-x/b_i) \quad (i = 1),$$

$$B_i = B_{(i-1)} \exp(-(x - x_{(i-1)})/b_i)(i > 1) \quad (7)$$

$$h_i = h_0 \exp(x(a_i - b_i)/a_i b_i) \quad (i = 1),$$

$$h_i = h_{(i-1)} \exp((x - x_{(i-1)})(a_i - b_i)/a_i b_i)(i > 1) \quad (8)$$

where A_i, B_i and h_i are the cross-sectional area, width and depth at location x from the mouth, respectively, A_0, B_0 and h_0 are the area, width and depth at the mouth, i represents the reach number (i = 1, 2, 3, ⋯, beginning from the mouth), a_i and b_i are the area and width convergence length for reach i, $x_{(i\text{-}1)}$ is the inflection point, and $A_{(i\text{-}1)}$, $B_{(i\text{-}1)}$ and $h_{(i\text{-}1)}$ are the cross-sectional area, width and depth, respectively, at the inflection point.

The cross-sectional average salt balance equations for High Water Slack (HWS), Low Water Slack (LWS) and Tidal Average (TA) situations can be written as:

$$S - S_f = c(\partial S/\partial x) \quad (9)$$

where S is the steady state salinity for three different states of HWS, LWS or TA, and S_f is the fresh water salinity. The coefficient c is an x-dependent coefficient equal to the ratio between the dispersion coefficient and the freshwater velocity:

$$c = (A/Q_f)D \quad (10)$$

where Q_f is the river discharge, which is negative since the positive x-axis points upstream, D is the dispersion coefficient for the HWS, LWS

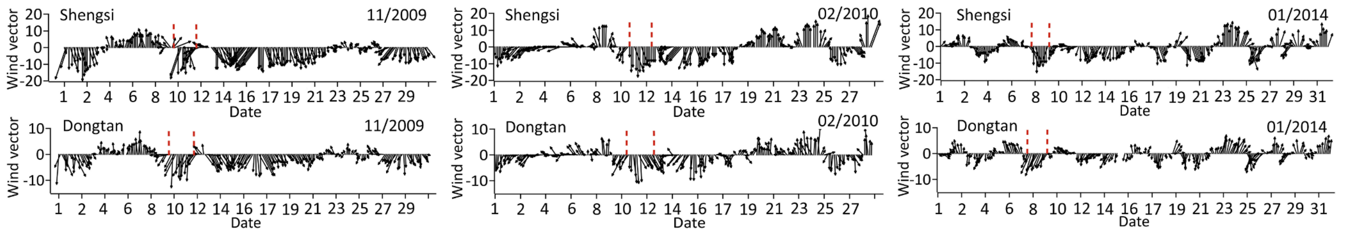

Fig. 4. Wind vectors at Shengsi and Dongtan stations in November 2009, February 2010, and January 2014. The dashed lines denote the strong wind periods corresponding with abnormal saline water intrusion.

or TA condition, which can be calculated by means of the following equation based on previous work by Van der Burgh (1972):

$$\partial D/\partial x = K(Q_f/A) \tag{11}$$

where K is Van der Burgh's coefficient, taken as a value between 0 and 1.

Combining Eqs. (9)–(11), the equation for the longitudinal variation of the salinity in the estuary is obtained:

$$(S - S_f)/(S_0 - S_f) = (D/D_0)^{(1/k)} \tag{12}$$

where S_0 is the boundary salinity at the estuary mouth (under the HWS, LWS or TA condition), and S_f is the salinity of the river water at the upstream boundary.

Integration of Eq. (11) in combination with an exponentially varying cross section yields the expression for the dispersion along the estuary:

$$D(x) = D_0\{1 - \beta_i(\exp(x/a_i) - 1)\}(i = 1),$$

$$D(x) = D_{(i-1)}\{1 - \beta_i(\exp((x - x_{(i-1)})/a_i) - 1)\} \quad (i > 1) \tag{13}$$

where:

$$\beta_i = -Ka_iQ_f/D_0A_0 \quad (i = 1), \quad \beta_i = -Ka_iQ_f/D_{(i-1)}A_{(i-1)} \quad (i > 1) \tag{14}$$

where β_i is the dispersion reduction rate at reach i for HWS, LWS or TA. $D_{(i-1)}$ is the dispersion coefficient at the inflection point for HWS, LWS, or TA. D_0 is the boundary condition at the estuary mouth ($x = 0$) for the HWS, LWS or TA condition, which can be calculated by means of the following predictive equation.

Based on observations in real estuaries, a predictive expression for the dispersion $D_0{}^{HWS}$ was obtained by Savenije (2005):

$$D_0^{\text{HWS}} = 1400(E_0 \upsilon_0 h_0/a)N_R^{0.5} \tag{15}$$

where N_R is the Estuarine Richardson number, which is defined as:

$$N_R = (\Delta\rho/\rho)(ghQ_f T/A_0E_0\upsilon_0^2) \tag{16}$$

where ρ is the density at the mouth, and Δρ is the density difference between ocean and river water. T is the tidal period; E_0 and υ_0 are the tidal excursion and tidal velocity amplitude at the estuary mouth respectively, $E_0 = \upsilon_0 T/\pi$.

Based on Lagrangean reasoning, $D_0{}^{TA}$ and $D_0{}^{LWS}$ can be computed as (Savenije, 1989):

$$D_0^{\text{TA}} = D^{\text{HWS}}(x = E/2)\exp(-E/2a) \tag{17}$$

$$D_0^{\text{LWS}} = D^{\text{HWS}}(x = E)\exp(-E/a) \tag{18}$$

where $D^{\text{HWS}}(x)$ is determined with Eqs. (13)–(16), and E is the tidal excursion.

Using the above equations the longitudinal salinity distribution in the estuary can be calculated for HWS, LWS, or TA.

3.2.2. Determination of the input parameters

The topographical parameters a_i and b_i are determined by means of fitting topographic data to the Eqs. (6)–(8). The Van der Burgh's coefficient K is an important parameter, which is obtained by calibrating the computed saline water intrusion curve against the measurements. It is usually regarded as constant independent of river discharge and tide. The tidal velocity amplitude at the estuary mouth υ_0 was determined based on measurements. The tidal excursion E_0 was calculated based on equation$E_0 = \upsilon_0 T/\pi$. Then, with the salinity (at the mouth) and the river discharge input, the longitudinal salinity distribution along the channel can be calculated based on equations (12)-(18). The model was calibrated using measurements on 1–2 January 2014.

4. Results

4.1. Variation trend and correlation of strong wind events and saline water intrusion in winter half year

The previous studies were mostly based on the wind conditions at Dongtan station. Fig. 4 shows the wind vectors at Shengsi and Dongtan stations in November 2009, February 2010, and January 2014. The wind directions at two stations were basically accordant, but the wind speeds at Shengsi were larger. On 10–12 November 2009, 11–12 February 2010, and 8–9 January 2014, three periods during which abnormal saline water intrusion occurred, the winds were mostly from north or northeast, with the speeds continuously exceeding 10 m/s and a maximum of higher than 15 m/s at the Shengsi station. On 10–12 November 2009, not only the northerly winds but also the northeasterly winds were dominant; they often occurred together during a single strong wind event. Because there is a lack of long-term data at the Dongtan station, the statistics of strong northerly and northeasterly wind events at the Shengsi station for winter half year were used for analyzing the variation trend and correlation with the saline water intrusion. Here a strong wind event is defined as: all wind speeds > = 10 m/s with a maximum > = 15 m/s, and the duration > = 12 h.

The Chenhang reservoir is located at the South Branch, supplying freshwater for Shanghai. Salinity here is controlled by the dispersion of saline water that originates from the North Branch. As such, the situation of saline water intrusion at Chenhang represents an index for saline water intrusion in the North Branch. According to statistics for the period 1994–2008, saline water intrusion at Chenhang was weak before 1999, but it had dramatically increased since 1999 both in terms of frequency and duration (plot a in Fig. 5). It can be seen from plots b and c of Fig. 5 that the frequencies and durations of strong northerly and northeasterly wind events had similar variation trend in the same period 1994–2008, low in the 1990 s, but increased dramatically after 1999 for the events with duration both less than 24 h and more than 24 h.

Fig. 6 shows the good correlation of frequencies between saline water intrusion and strong northerly and northeasterly wind events in 1994–2008. For the events with duration longer than 12 h, the correlation coefficient was 0.85. This suggests that the increase of strong northerly and northeasterly wind events may be one factor inducing the increase of saline water intrusion in the North Branch of the Yangtze Estuary after 1999.

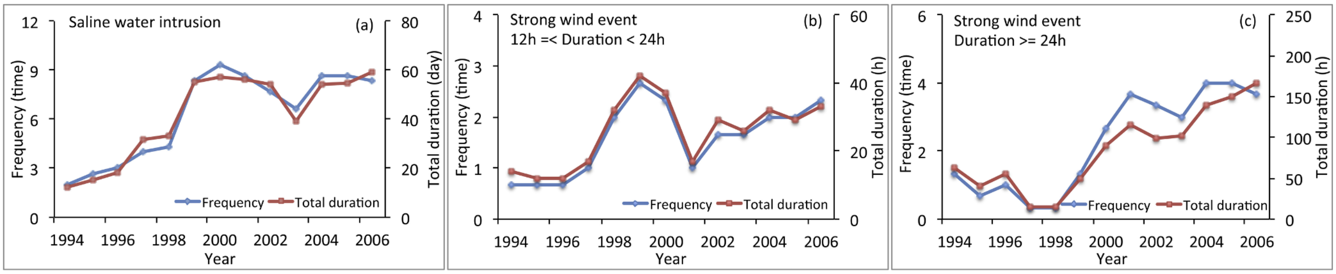

Fig. 5. Variations of saline water intrusion at Chenhang reservoir (a) and strong northerly and northeasterly wind events at Shengsi station in winter half year (b and c) in 1994–2008. The values in the curves are 3-year moving average.

4.2. Processes of strong northerly and northeasterly winds increasing saline water intrusion

Water depth, tidal range, tidal currents, and freshwater inflow are the main factors controlling saline water intrusion. For the North Branch of the Yangtze Estuary, these are all affected by the condition of strong northerly and northeasterly winds.

4.2.1. Water level setup

The net water level setup and setdown at the Qinglonggang station based on EMD, subtidal water levels based on low-pass filter, and wind conditions in November 2009, February 2010, and January 2014 are presented in Fig. 7. The net water level setup and setdown based on EMD (plots d, e, f) were in accordance with the variation of subtidal water levels (plots a, b, c), and also basically corresponded with the variation of wind conditions (plots g-o). The water level setups mostly corresponded with the northerly and northeasterly winds, which was in accordance with the decrease of temperature influenced by cold air particularly for the strong winds (plots g-i). During 10–12 November 2009 (neap tide), 11–12 February 2010 (intermediate tide), and 8–9 January 2014 (neap tide), the three periods during which abnormally strong saline water intrusion occurred, the water levels all set up dramatically corresponding with strong northerly and northeasterly winds. The highest wind speed 20 m/s agreed with the highest water level setup of 0.55 m during 10–12 November 2009 in the three periods.

In addition, during 16–17 November 2009 (quasi-spring tide) water levels surged dramatically as well, corresponding with the strong northeasterly winds with a maximum speed of 18 m/s at Shengsi. Fig. 2 shows that the salinity values around 17 November 2009 was much higher than those during the previous spring tide (around 3–4 November) at the Chongxi station, although on that day the tidal range was smaller and the corresponding Yangtze River discharge was relatively large. The salinity increase was probably induced by the strong northeasterly winds as well. Water level set up implies water depth increase, which is a factor inducing increase of saline water intrusion.

4.2.2. Limited change of tidal range

The setup and setdown of tidal range at the Qinglonggang station in November 2009, February 2010 and January 2014 based on EMD are presented in plots a-c of Fig. 8, which generally corresponded with the variations of subtidal tidal range in plots d-f. In the subtidal tidal ranges because the difference between spring tide and neap tide is large, the small changes were not obvious particularly during neap tide. The setup and setdown of tidal range resulted from the change of water level, depending on the water level setup or setdown during flood and ebb. The changes of tidal range were generally small, because the water level set up or set down during both flood and ebb.

During the several strong wind events, the tidal ranges had both setups and setdowns. The relatively large setups and setdowns usually occurred at the beginning or end of the events, resulting from the sudden setup and setdown during flood or ebb, with a maximum setup of 0.16 m and a maximum setdown 0.25 m in November 2009 and January 2014. On 11–12 February 2010, the situation was slightly different. The tidal range set up during the whole event with a maximum of 0.25 m, which can be seen also from the subtidal tidal ranges (plot e). This is likely the result of the larger setups during the flood phase of the tide than during the ebb.

4.2.3. Flood-tide current enhanced and ebb-tide current reduced

In the North Branch of the Yangtze Estuary the tidal current velocity during flood tide is usually larger than during ebb tide in spring tide. In neap tide the tidal current velocity during flood tide is generally smaller than during ebb tide. However, on 8 January 2014 (neap tide) during strong northerly winds the tidal current velocities during flood tide were larger than during ebb tide at locations B1, B2 and B3 (Fig. 9). Particularly in the first tidal cycle of B1, the much smaller velocities during ebb tide can be easily seen. The strong winds began at 04:00 or 05:00, i.e., the velocities during the ebb tide were affected by strong winds. In the second tidal cycle of B2, the maximum velocity during the ebb was larger than during the flood, which corresponded with the smaller tidal range and much weaker winds. This observation suggests that the velocities on 8–9 January 2014 were affected by the strong

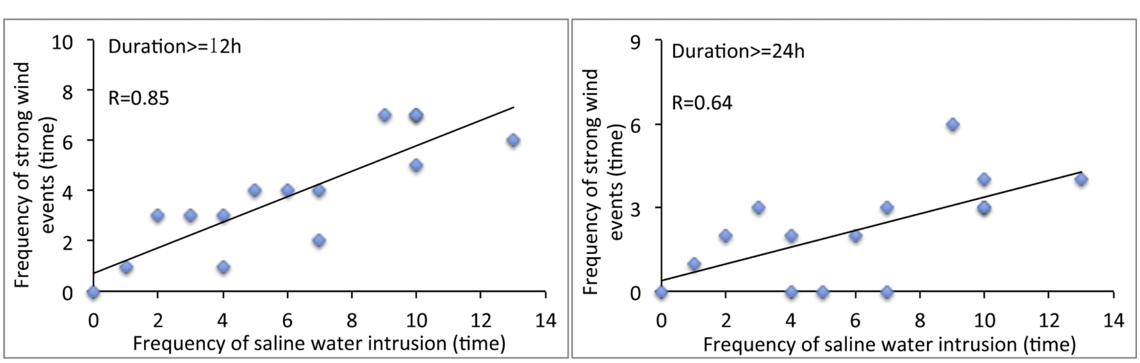

Fig. 6. Correlation between saline water intrusion at Chenhang reservoir and strong northerly and northeasterly wind events at Shengsi station in 1994–2008. R is correlation coefficient.

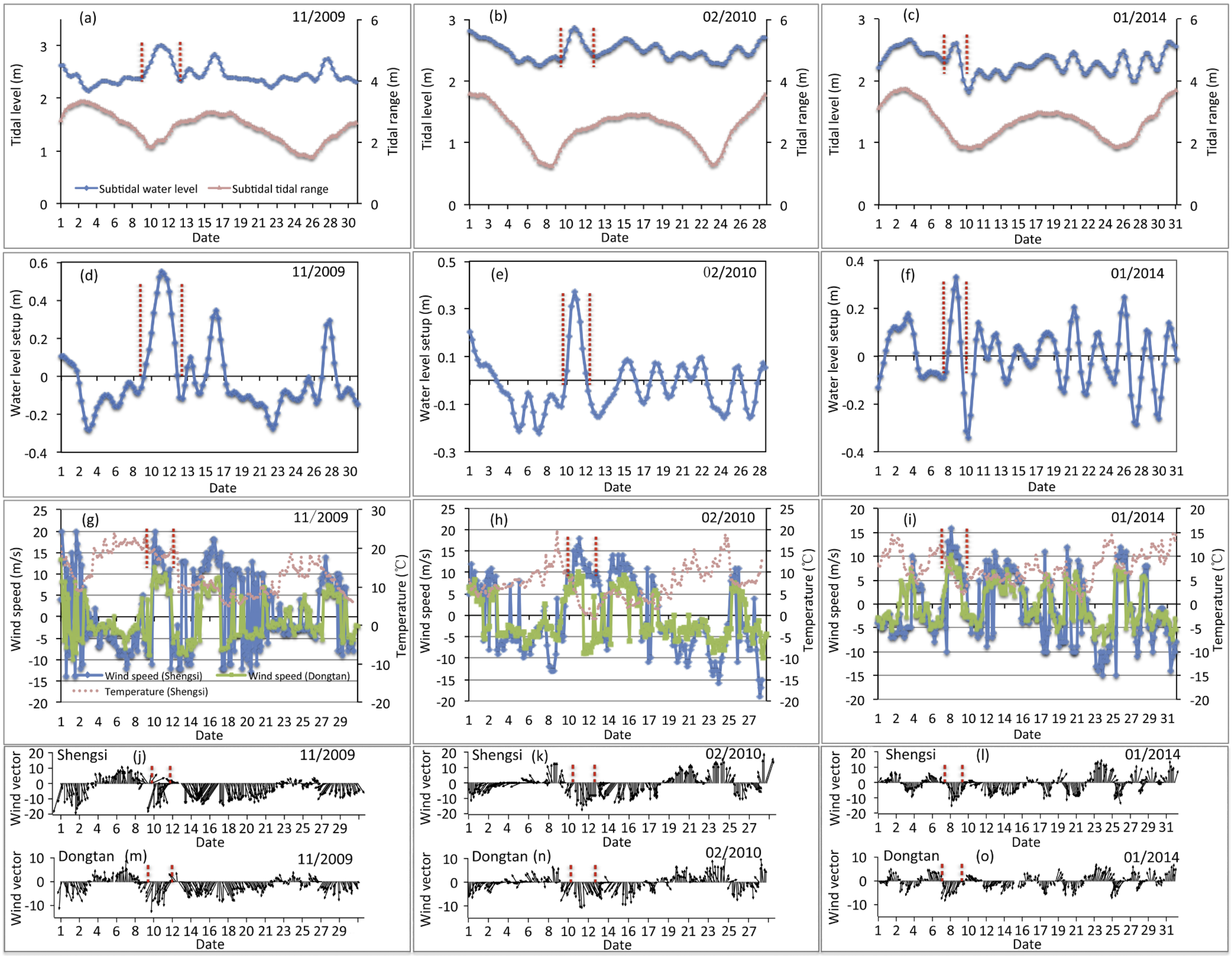

Fig. 7. Water level setup and setdown at the Qinglonggang station, compared with wind observations in November 2009, February 2010, and January 2014. Diamonds and triangles in plots a, b, c represent subtidal water levels and tidal ranges respectively. Plots d, e, f show the net water level setup and setdown. Plots g, h, i show the wind speeds with positive values representing northerly and northeasterly winds, and temperature. Plots j-o show the wind vectors. The dashed straight lines denote the three periods during which the abnormally strong saline water intrusion occurred.

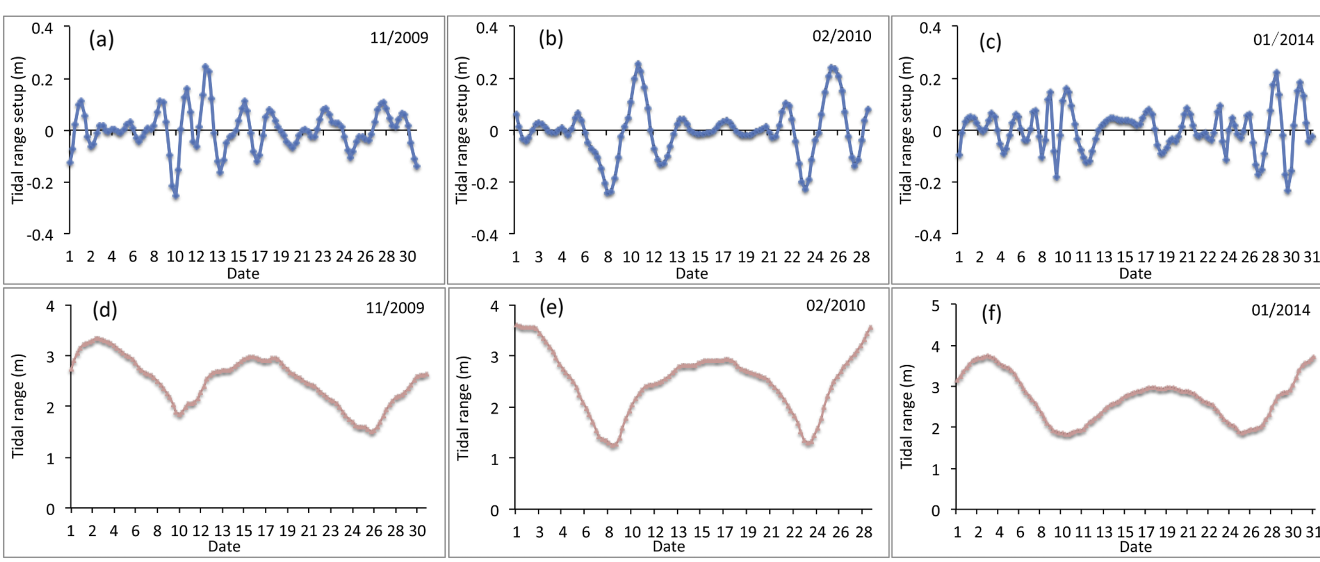

Fig. 8. Tidal range setup and setdown at the Qinglonggang station in November 2009, February 2010, and January 2014. Plots d-f show the subtidal tidal ranges.

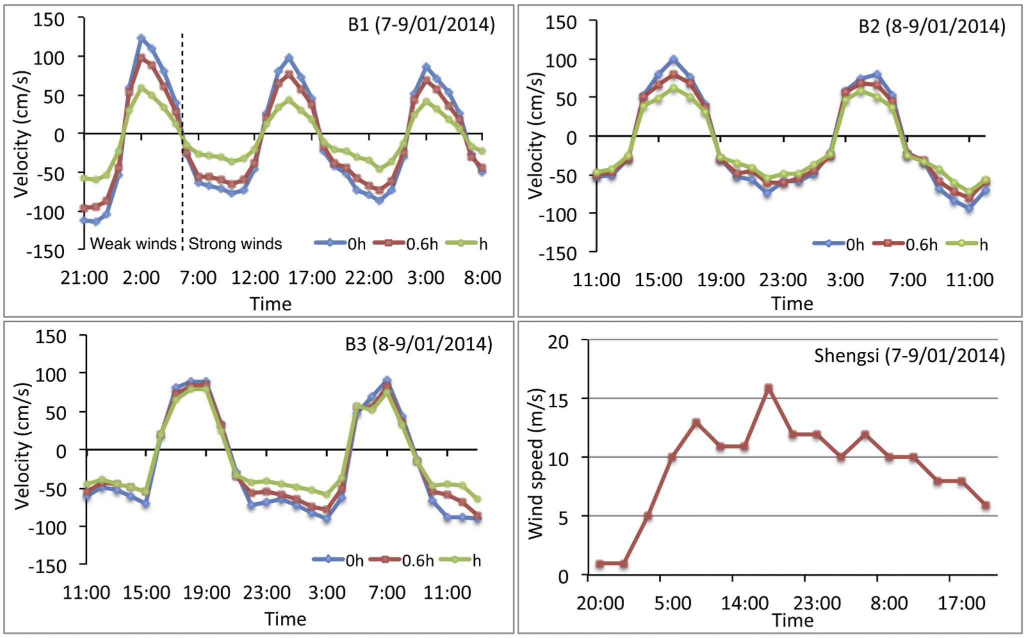

Fig. 9. Variations of tidal current velocity at locations B1, B2 and B3 of the North Branch, compared with wind speeds at the Shengsi station on 7–9 January 2014. The positive and negative velocities represent flood tide and ebb tide respectively. The tidal current velocities were measured with interval of 1 h, and the wind speeds were observed with interval of 3 h. 0 h, 0.6 h, and h in the legend represent surface, 60% depth, and bottom in the vertical profile.

northerly winds, whereby the flood-tide velocities increased and the ebb-tide velocities decreased. This induced the increase of saline water intrusion. In November 2009 and February 2010 no measured current data were available.

4.2.4. Decrease of freshwater inflow

Due to the special topography, the ratio of freshwater inflow into the North Branch is very small, less than 1% of the Yangtze River discharge in recent years (Chen and Chen, 2003; Yu et al., 2003; Tan and Wang, 2004; Zhang et al., 2011). The saline water intrusion in the North Branch is sensitive to the freshwater inflow, particularly during dry season. The strong northerly and northeasterly winds set up water levels, strengthen flood currents, and reduce ebb currents, which block freshwater inflow into the North Branch and further downstream. This may be an important mechanism inducing abnormally strong saline water intrusion during strong northerly and northeasterly winds on 10–12 November 2009, 11–12 February 2010 and 8–9 January 2014.

The longitudinal salinity distributions along the North Branch on 1–2 (spring tide) and 8–9 (neap tide) January 2014 were computed based on the analytical model. During neap tide, water depth, tidal velocity amplitude, and ratio of freshwater inflow were possibly influenced by strong winds, which were considered in the calculation of salinity. Water depth h_i was set to increase 0.3 m based on the net water

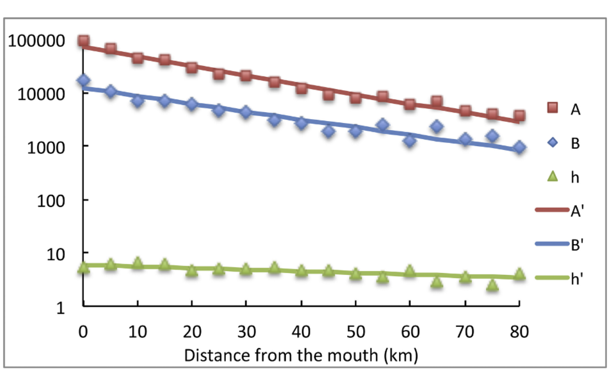

Fig. 10. Topography of the North Branch, showing cross-sectional area A (m^2), the width B (m), and the depth h (m) (squares, diamonds, and triangles represent observations, and the drawn lines represent the exponential equations (6)-(8)).

level setup. The tidal velocity amplitude at the estuary mouth υ_0 was determined based on observations. The topography of the North Branch, parameters used in the model, and computed salinity are shown in Fig. 10, Table1 and Fig. 11, respectively.

Fig. 11 shows that the computed salinity agreed with the measured salinity well except for the low salinity at B3 in the upper reach during neap tide. For the computed results the input freshwater inflow into the North Branch during neap tide is much smaller than for spring tide (Table1). The absence of high-low variations of salinity during flood and ebb tides, almost equal high salinity in the middle and lower reaches, and very high salinity during flood tide in the upper reach all confirmed very small freshwater inflow. However, there was no much difference between the corresponding Yangtze River discharges during spring and neap tides (Fig. 2, Table1). If the ratio of freshwater inflow during neap tide were not changed, the same as the spring tide, the salinity would be much lower (dashed lines in Fig. 11). Only the high salinity at B1 in the lower reach and low salinity at B3 in the upper reach can fit the measurements. This suggests the effect of strong northerly winds inducing a decrease of freshwater inflow into the North Branch.

The poor agreement between computed results and measurements for the low salinity at B3 in the upper reach during neap tide is due to the fact that B3 is close to the South Branch, where the salinity is largely affected by freshwater during the ebb. During the flood the tidal current is dominant, the salinity can reach a high value, which is why the saline water can spill over into the South Branch. If the North Branch were a single channel estuary, the saline water intrusion could reach around 130 km during the flood, and the low salinity at B3 would be much higher for the same freshwater inflow.

4.3. Mechanism of wind forcing on saline water intrusion

The effects of wind on the hydrodynamics and saline water intrusion may come from two sides: the effects of remote winds over the continental shelf, and the effects of local winds over the estuary. The alongshore winds over the continental shelf could generate Ekman transport toward or off the estuary and coastal area, inducing coastal sea level fluctuations and subtidal exchange between the estuarine and shelf waters (Snedden et al., 2007; Ralston et al., 2008). In the Yangtze Estuary, the events of abnormal salinity increase in the North Branch all correspond with alongshore winds, i.e. the northerly and northeasterly

Table 1
Parameters used in the model.

Tidal condition	A_0 (m^2)	B_0 (m)	h_0 (m)	a (km)	b (km)	K	Q_f (m^3/s)	RFI (%)	S_0	v_0 (m/s)	E_0 (m)
Spring tide	70,000	12,000	5.8	25	30	0.3	13,000	0.13	30.5	1.5	21,210
Neap tide	73,000	12,000	6.1	26	30	0.3	12,000	0.02	29.5	0.9	12,726

Note: Q_f refers to the discharge of the Yangtze River. RFI represents the ratio of freshwater inflow into the North Branch.

winds. The resulted Ekman transport by winds over the continental shelf forces seawater towards the estuary mouth. This process results in water level setup outside the estuary mouth and an enhanced seawater transport into the estuary, which has been proposed by Wu et al. (2010) and Li et al. (2012) based on numerical experiments. In addition to pumping more seawater into the estuary during flood tide, this process blocks water out of the estuary during ebb tide, inducing water level setup during both flood and ebb tides, the increase of current velocity during flood tide, and decrease of velocity during ebb tide.

The local northeasterly winds are exactly parallel to the upper reach of the North Branch, which could play some role as well. The numerical experiment by Li et al. (2012) confirmed that the water mass spilling over into the South Branch from the North Branch under a northeasterly wind condition was larger than under a northerly wind condition. However, it can be seen from Fig. 12 that the wind speeds inside the estuary were much smaller than outside during the strong winds event of 8–9 January 2014, affected by the terrestrial topography, although the wind directions were similar. The wind speeds at B2 and B3 in the middle and upper reaches were smaller than 4 m/s in half and even longer period of the strong winds event. This suggests that the effect of local winds is limited. The Shengsi station outside the estuary is also a land-based station on the Shengsi island. The winds over the sea should be stronger. This also suggests that the effect from remote winds was dominant.

5. Discussions

5.1. Effects of wind on hydrodynamics

Song et al. (2011) studied the effects of wind on water level and tidal range at Qinglonggang station based on numerical experiments and multi-years average wind conditions at half-month mean level. Their results indicate that the winds have small effect on water level and almost no effect on tidal range. The water level setups influenced by the northerly winds are generally smaller than 0.05 m. Our results based on observations show that during the strong northerly and northeasterly winds the water level set up dramatically, with a maximum of 0.55 m at the Qinglonggang station during 10–12 September 2009. This dramatic water level setup can occur on neap, intermediate or spring tide. This result is different from the numerical experiment result by Song et al. (2011), too. Their result indicates that the water level setup is relatively strong during neap tides, but no obvious setup or even setdown occurs during spring tides, as a result of the same northerly wind conditions. On neap tides the tidal intensity is weak, so the effects of wind could be larger. On spring tides, the situation is vice versa. However, observations show that if the winds are strong, the effect of winds is obvious as well during spring tides, e.g., 16–17 November 2009 with a maximum wind speed of 18 m/s at the Shengsi station.

As to the tidal range, our results indicate that the variations during strong winds are not much with both setup and setdown. However, the magnitude is much larger than the result from Song et al. (2011). In some cases, relatively large setups occurred, such as those on 11–12 February 2010 with a maximum of 0.25 m. The relationship between wind and hydrodynamics should be nonlinear, so additional work is needed to confirm the results including the variations of tidal current velocity which were based on a limited data set.

5.2. Mechanisms related to wind forcing

For the effects of wind on subtidal variability of hydrodynamics and saline water intrusion, the Ekman transport resulting from remote alongshore winds is believed to be the main mechanism in many estuaries such as Great South Bay (Wong and Wilson, 1984), Delaware Estuary (Wong and Garvine, 1984; Ross et al., 2015), Mississippi River Deltaic estuary (Snedden et al., 2007), Keum River Estuary (Son et al., 2007), Chesapeake Bay (Guo and Valle-Levinson, 2008), northern Gulf of Mexico Estuary (Kim and Park, 2012), and Narragansett Bay estuary (Pfeiffer-Herbert et al., 2015). In the Yangtze Estuary this mechanism was also proposed by Wu et al. (2010) and Li et al. (2012). Garvine (1985) believed that the effect of remote winds is larger than local winds because most estuaries are short relative to the low subtidal estuarine wave length. Our results indicate that the remote winds outside the estuary are much stronger than the local winds over the estuary, which may represent another reason for the dominance of remote effects. This result also suggests that the replacement of local winds by

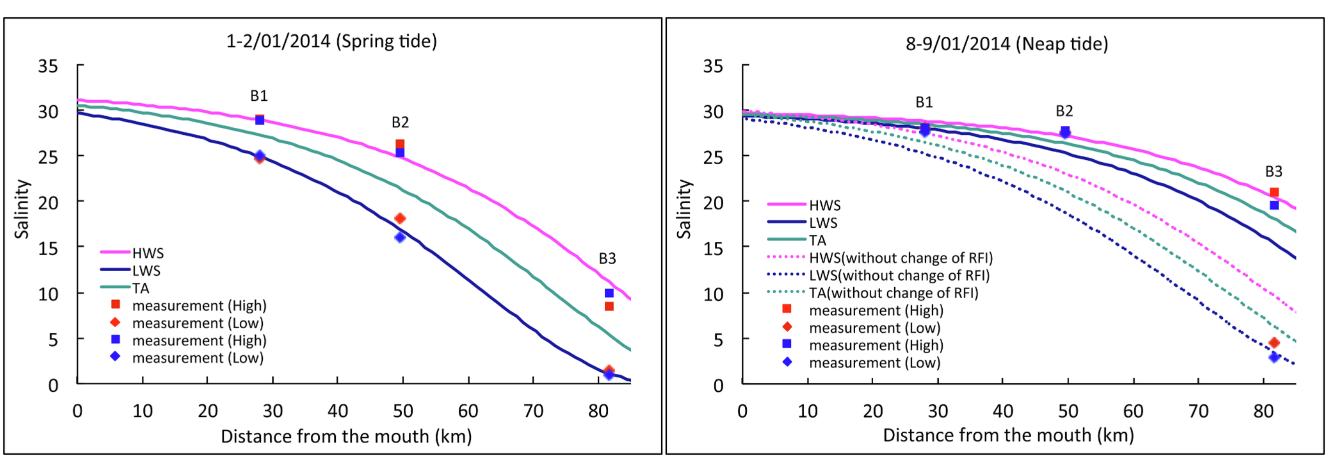

Fig. 11. Computed salinity distribution along the North Branch on 1–2 and 8–9 January 2014 based on analytical model, compared with measurements. RFI in the legend of the right plot means ratio of freshwater inflow.

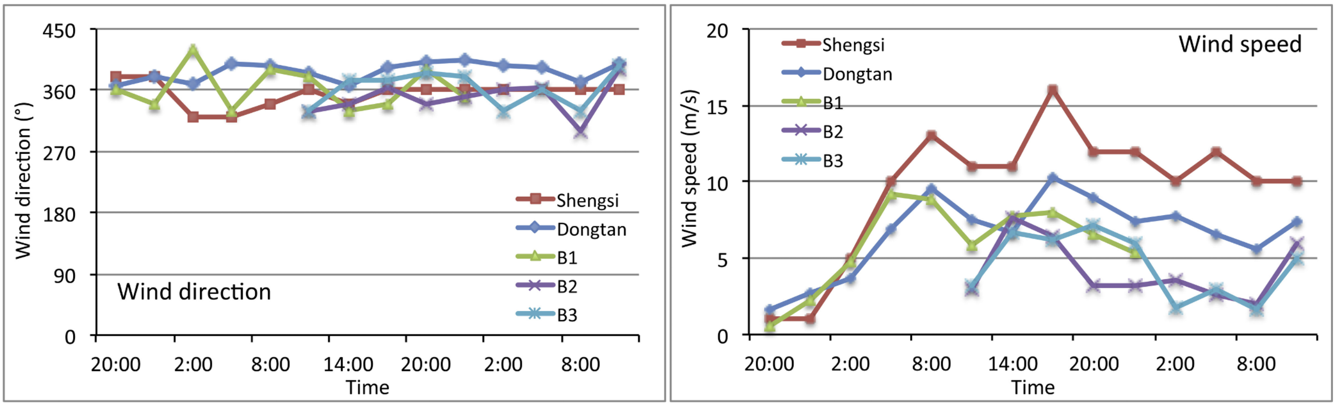

Fig. 12. Wind directions and speeds at stations Shengsi, Dongtan, B1, B2 and B3 on 7–9 January 2014.

remote winds or replacement of remote winds by local winds in some previous research is unreasonable.

In micro-tidal estuaries, stratification is more common whereby intrusion of seawater takes place in the form of a salt wedge. In that case, gravitational circulation and nonlinear pumping-effect are the main mechanisms (Zyryanov, 2013; Zyryanov et al., 2015). In those estuaries, the along-channel local winds could apparently affect the saline water intrusion. Down-estuary and up-estuary winds increase and curb the circulation, respectively, resulting in an increase and decrease of saline water intrusion, as is the cases in the Lower Patos Lagoon Estuary (Costa et al., 1988) and the Pamlico River Estuary (Xu et al., 2008).

In addition, outside the Yangtze Estuary there are alongshore currents from the north in winter season. During the strong northerly winds, the alongshore currents are intensified (Riedlinger and Jacobs, 2000). And some studies suggest that the water level setup forced by strong winds can propagate southward in the form of Kelvin waves (Ko et al., 2003; Yang et al., 2016). These two factors may also induce the water level setup at the estuary mouth, influencing the hydrodynamics and saline water intrusion.

6. Conclusions

The statistics of the 1994–2008 data sets show that the frequency and duration of saline water intrusion in the North Branch of the Yangtze Estuary were weak in the 1990s, but they had dramatically increased since 1999. The strong northerly and northeasterly wind events around the estuary during cold outbreaks in winter half year show the similar variation trend in both frequency and duration: low in the 1990s but increased dramatically after 1999. In addition to this agreement in trend, the correlation between strong wind events and saline water intrusion is also significant. This suggests that the increase of strong northerly and northeasterly wind events may be one of the factors inducing the increase of saline water intrusion in the North Branch of the Yangtze Estuary.

In situ observations show that strong northerly and northeasterly winds can induce dramatic water level setup in the North Branch of the Yangtze Estuary, which can occur in neap, intermediate, or spring tide. The tidal range is relatively less affected due to the water level setup during both flood and ebb tides. The current velocities are also affected, whereby the flood-tide velocities increased and ebb-tide velocities decreased. In addition, the results of the analytical saline water intrusion model suggest that the freshwater inflow into the North Branch decreases considerably. These changes in combination cause the intensified saline water intrusion.

During strong northerly and northeasterly winds, Ekman transport from remote winds over the continental shelf areas forces seawater towards the coastal area and estuary mouth, which induces water level setup at the mouth, pumping more seawater into the estuary. This should be a primary mechanism for the change of hydrodynamics and increase of saline water intrusion. The much stronger winds outside than inside the estuary also suggest the dominant effect of remote winds.

Acknowledgements

We thank the National Centers for Environmental Information (NCEI), the State Key Laboratory of Estuarine and Coastal Research, the Jiangsu Province Hydrology and Water Resources Investigation Bureau, and the Hydrological Administration of Anhui Province for providing the wind and temperature data sets at the Shengsi station, the wind data at the Dongtan station and the bathymetric data of the North Branch, tidal levels at the Qinglonggang station, and river discharges at the Datong station, respectively. We appreciate professor Yaping Wang's help during data processing. This study was supported by the National Natural Science Fundation of China (NSFC-NWO-RCUK joint project, Grant No. 51761135023). We are grateful to the referees for the valuable comments and suggestions on the original manuscript of the paper.

References

Bolaños, R., Brown, J.M., Amoudry, L.O., Souza, A.J., 2013. Tidal, riverine, and wind influences on the circulation of a macrotidal estuary. J. Phys. Oceanogr. 43, 29–50.
Cao, Y., Chen, J.Y., Zhang, E.F., Chen, S.L., Cao, W.C., 2006. Influence of Three Gorge reservoir filled with water on fresh water resource in the Yangtze River estuary. Adv. Water Sci. 17, 554–558 (in Chinese).
Chen, J.Y., Chen, S.L., 2003. Variations of ecology and environment in the Yangtze Estuary and suggestions on regulating the estuary. Water Resour. Hydropower Eng. 34 (1), 19–25 (in Chinese).
Chen, W., Su, J.L., 1991. Mechanisms of low frequency fluctuations of water levels in the Hangzhou Bay. Acta Oceanol. Sin. 13 (1), 1–12 (in Chinese).
Costa, C.S.B., Seeliger, U., Kinas, P.G., 1988. The effect of wind velocity and direction on the salinity regime in the Lower Patos Lagoon estuary. Ciência e Cultura 40 (9), 909–912.
Garvine, R.W., 1985. A simple model of estuarine subtidal fluctuations forced by local and remote wind stress. J. Geophys. Res. 90 (C6), 11945–11948.
Giardino, D., 2009. Analysis of the physical forcing mechanisms influencing salinity transport for the lower St. Johns River. Master thesis. Department of Civil and Environmental Engineering in the College of Engineering and Computer Science. University of Central Florida, Orlando, Florida.
Gu, Y.L., Wu, S.P., Le, Q., 2003. Impact of saline water intrusion in the North Branch of the Yangtze Estuary on the freshwater-supply areas. Yangtze River 34 (4), 1–3 (in Chinese).
Guo, X., Valle-Levinson, A., 2008. Wind effects on the lateral structure of density-driven circulation in Chesapeake Bay. Cont. Shelf Res. 28 (17), 2450–2471.
Huang, N.E., Shen, Z., Long, S.R., Wu, M.C., Shih, E.H., Zheng, Q., Tung, C.C., Liu, H.H., 1998. The empirical mode decomposition method and the Hilbert spectrum for non-stationary time series analysis. Proceed. R. Soc. London A. 454, 903–995.
Kim, C.K., Park, K., 2012. A modeling study of water and salt exchange for a micro-tidal, stratified northern Gulf of Mexico estuary. J. Mar. Syst. 96–97, 103–115.
Ko, D.S., Preller, R.H., Jacobs, G.A., Tang, T.Y., Lin, S.F., 2003. Transport reversals at Taiwan Strait during October and November 1999. J. Geophys. Res. 108 (C11), 3370. https://doi.org/10.1029/2003JC001836.
Li, C.Y., Roberts, H., Stone, G.W., Weeks, E., Luo, Y.X., 2011. Wind surge and saltwater

intrusion in Atchafalaya Bay during onshore winds prior to cold front passage. Hydrobiologia 658, 27–39.
Li, L., Zhu, J.R., Wu, H., 2012. Impacts of wind stress on saltwater intrusion in the Yangtze Estuary. Sci. China Earth Sci. 55 (7), 1178–1192.
Manca, F., Capelli, G., Vigna, F.L., Mazza, R., Pascarella, A., 2014. Wind-induced salt-wedge intrusion in the Tiber river mouth (Rome–Central Italy). Environ. Earth Sci. 72, 1083–1095.
Pfeiffer-Herbert, A.S., Kincaid, C.R., Bergondo, D.L., Pockalny, R.A., 2015. Dynamics of wind-driven estuarine-shelf exchange in the Narragansett Bay estuary. Cont. Shelf Res. 105, 42–59.
Ralston, D.K., Geyer, W.R., Lerczak, J.A., 2008. Subtidal salinity and velocity in the Hudson River Estuary: observations and modeling. J. Phys. Oceanogr. 38, 753–770.
Reyes-Merlo, M.Á., Díez-Minguito, M., Ortega-Sánchez, M., Baquerizo, A., Losada, M.Á., 2015. On the relative influence of climate forcing agents on the saline intrusion in a well-mixed estuary: Medium-term Monte Carlo predictions. J. Coastal Res. Special Issue 65, 1200–1205.
Riedlinger, S.K., Jacobs, G.A., 2000. Study of the dynamics of wind-driven transports into the Yellow Sea during winter. J. Geophys. Res. 105 (C12), 28695–28708.
Ross, A.C., Najjar, R.G., Li, M., Mann, M.E., Ford, S.E., Katz, B., 2015. Sea-level rise and other influences on decadal-scale salinity variability in a coastal plain estuary. Estuar. Coast. Shelf Sci. 157, 79–92.
Savenije, H.H.G., 1986. A one-dimensional model for salinity intrusion in alluvial estuaries. J. Hydrol. 85, 87–109.
Savenije, H.H.G., 1989. Salt intrusion model for high-water slack, low-water slack and mean tide on spread sheet. J. Hydrol. 107, 9–18.
Savenije, H.H.G., 2005. Salinity and Tides in Alluvial Estuaries. Elsevier, Amsterdam.
Simionato, C.G., Meccia, V.L., Guerrero, R., Dragani, W.C., Nuñez, M., 2007. Rio de la Plata estuary response to wind variability in synoptic to intraseasonal scales: 2. Currents' vertical structure and its implications for the salt wedge structure. J. Geophys. Res. 112, C07005. https://doi.org/10.1029/2006JC003815.
Snedden, G.A., Cable, J.E., Wiseman, W.J., 2007. Subtidal sea level variability in a shallow Mississippi River Deltaic estuary, Louisiana. Estuar. and Coast. 30 (5), 802–812.
Son, Y.T., Lee, S.H., Kim, C.S., Lee, J.C., Lee, G.H., 2007. Surface current variability in the Keum River Estuary (South Korea) during summer 2002 as observed by high-frequency radar and coastal monitoring buoy. Cont. Shelf Res. 27, 43–63.
Song, Y.G., Zhu, J.R., Wu, H., 2011. Spatial and temporal variations and mechanism of the tidal level and range in the North Branch of the Changjiang Estuary. J. East China Normal Univer. (Nat. Sci.). 6, 10–19 (in Chinese).
Tan, P.L., Wang, H.Y., 2004. The analysis of Three Gorges project alleviating salt tide intrusion in the Yangtze Estuary. China Three Gorges Construct. 5, 29–31 (in Chinese).
Tang, J.H., Xu, J.Y., Zhao, S.W., Liu, W.Y., 2011. Research on saltwater intrusion of the South Branch of the Changjiang Estuary based on measured data. Resour. Environ. Yangtze Basin 20 (6), 677–684 (in Chinese).
Van der Burgh, P., 1972. Ontwikkeling van een methode voor het voorspellen van zoutverdelingen in estuaria, kanalen en zeeen. Rijkwaterstaat Rapport 10–72 (in Dutch).
Wong, K., Moses-Hall, J.E., 1998. On the relative importance of the remote and local wind effects to the subtidal variability in a coastal plain estuary. J. Geophys. Res. 103 (C9), 18393–18404.
Wong, K., Garvine, R.W., 1984. Observations of wind-induced, subtidal variability in the Delaware Estuary. J. Geophys. Res. 89 (C6), 10589–10597.
Wong, K., Wilson, R.E., 1984. Observations of low-frequency variability in Great South Bay and relations to atmospheric forcing. J. Phys. Oceanogr. 14, 1893–1900.
Wu, Z., Huang, N.E., 2009. Ensemble empirical mode decomposition: a noise assisted data analysis method. Adv. Adapt. Data Anal. 1 (1), 1–41.
Wu, H., Zhu, J.R., Choi, B.H., 2010. Links between saltwater intrusion and subtidal circulation in the Changjiang Estuary: a model-guided study. Cont. Shelf Res. 30 (17), 1891–1905.
Xu, H.Z., Lin, J., Wang, D.X., 2008. Numerical study on salinity stratification in the Pamlico River Estuary. Estuar. Coast. Shelf Sci. 80, 74–84.
Xu, J.Y., Yuan, J.Z., 1994. The study about law of saltwater intrusion in the South Branch of the Yangtze Estuary. Hydrology 5, 1–5 (in Chinese).
Xue, P., Chen, C., Ding, P., Beardsley, R.C., Lin, H., Ge, J., Kong, Y., 2009. Saltwater intrusion into the Changjiang River: a model-guided mechanism study. J. Geophys. Res. 114, C02006. https://doi.org/10.1029/2008JC004831.
Yang, J.X., Yuan, F.C., Li, Z.M., Wu, X.R., 2016. Application of the EMD method in the storm surges at the coast of China. Marine Sci. Bull. 35 (2), 157–162 (in Chinese).
Yu, F.X., Song, Z.Y., Li, R.J., 2003. A 3-D hydrodynamical model for tidal current field of the Yangtze River Estuary. Trans. Oceanol. Limnol. 3, 14–23 (in Chinese).
Zhang, E.F., Chen, S.L., Liu, X.X., 2014. Observation and analysis of abnormal strong saltwater intrusion in the North Branch of the Yangtze Estuary. Marine Sci. Bull. 33 (5), 491–496 (in Chinese).
Zhang, E.F., Savenije, H.H.G., Chen, S.L., Chen, J.Y., 2012. Water abstraction along the lower Yangtze River, China, and its impact on water discharge into the estuary. Phys. Chem. Earth. 47–48, 76–85.
Zhang, E.F., Savenije, H.H.G., Wu, H., Kong, Y.Z., Zhu, J.R., 2011. Analytical solution for salt intrusion in the Yangtze Estuary, China. Estuar. Coast. Shelf Sci. 91, 492–501.
Zhao, B.R., Cao, D.M., 1987. Wintertime low frequency fluctuations of Chinese coastal sea-level in the Huanghai Sea and the East China Sea. Oceanologia et Limnologia Sin. 18 (6), 563–574 (in Chinese).
Zyryanov, V.N., 2013. Nonlinear pumping-effect in oscillation processes in geophysics. Water Resour. 40 (3), 243–253.
Zyryanov, V.N., Chebanova, M.K., Filatov, N.N., 2015. Seawater intrusion into river mouths. Water Resour. 42 (5), 616–626.